

# Light-Trapped Nanocavities for Ultraviolet Surface-Enhanced Raman Scattering

Yue Zeng,<sup>#</sup> Renxian Gao,<sup>#</sup> Jingyu Wang, Tien-Mo Shih, Guoya Sun,<sup>\*</sup> Jiasheng Lin, Yonglin He, Jiawei Chen, Da Zhan, Jinfeng Zhu, Weimin Yang, Peiwen Ren, Fangfei Jiao, and Zhilin Yang<sup>\*</sup>

 Cite This: *J. Phys. Chem. C* 2021, 125, 17241–17247

 Read Online

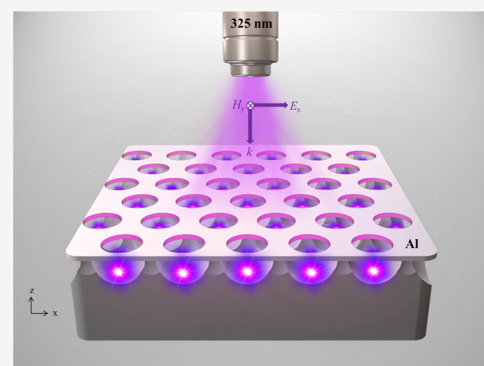
ACCESS |

 Metrics & More

 Article Recommendations

 Supporting Information

**ABSTRACT:** The fabrication of surface-enhanced Raman scattering (SERS) substrates with large areas, high activities, desirable uniformities, and aggregated hot spots evenly distributed in the UV (ultraviolet) region has been regarded as a formidable task. In the present work, by means of elaborate structure designs and material selections, we have fabricated periodic light-trapped nanocavities that have overcome the abovementioned difficulties. Specifically, a great amount of electromagnetic energy has been localized in nanocavities due to repeated reflections of the trapped incident light, thus re-amplifying abundant hot spots of the aluminum film. At an excitation wavelength of 325 nm, the acquisition of ultrahigh SERS enhancement factors ( $\geq 10^6$ ) has been successfully achieved, and signal intensities are uniformly distributed after repeated measurements. In the originally weak UV region, our nanostructure design and its associated mechanism may provide a guide for future SERS-related research.



## INTRODUCTION

As a powerful analytical tool with ultrahigh sensitivity and specificity, surface-enhanced Raman scattering (SERS)<sup>1–3</sup> has motivated a variety of applications in physics,<sup>4</sup> chemistry,<sup>5</sup> biology,<sup>6</sup> surface science,<sup>7</sup> materials science,<sup>8</sup> and other fields.<sup>9</sup> To construct effective SERS enhanced platforms, researchers have utilized noble metals, such as Au<sup>10,11</sup> and Ag,<sup>12,13</sup> to generate surface-plasmon-resonance (SPR) hot spots that span visible and near-infrared wavelengths. In the ultraviolet (UV) region, however, cost-effective SERS substrates that feature large-scale, unsophisticated preparation methods, numerous hot spots, great uniformity, and high activity remain lacking.

Appropriate structure designs and material selections of substrates play crucial roles in producing hot spots with strong electromagnetic fields in the UV regime. Fortunately, in the visible interval, pioneering researchers have already accomplished designing structures based on resonance coupling effects,<sup>14–16</sup> resonant cavity effects depending on standing waves,<sup>17</sup> field focusing effects caused by tips,<sup>18,19</sup> and lightning rod effects<sup>20</sup> among others, providing a valuable guide for extension studies to the UV regime.<sup>21,22</sup> Nonetheless, UV-SERS substrates, which have been fabricated via electrochemical oxidation reduction cycle electrodeposition or magnetron sputtering in transition-metal systems (Ni, Ru, Rh, and Co),<sup>23–26</sup> may sometimes exhibit low activities and weak signal uniformities.

Generally, as an appropriate material that can effectively support the resonance of high intensity surface plasmons in the UV region, Al<sup>27–30</sup> has greatly attracted researchers' interest.

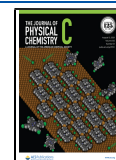
For instance, Löffler et al.<sup>31</sup> have fabricated Al nanoparticle arrays by extreme ultraviolet lithography, which yields large-area, high-throughput UV-SERS substrates. Also, the preparation of large-scale high-enhancement-factor substrates has been achieved by controlled self-assembled Al nanostructures by Li et al.<sup>32</sup> Simple template self-assembled polystyrene spheres<sup>33</sup> and nano-imprint lithography<sup>34</sup> are used to fabricate reusable and mass-produced UV-SERS substrates. However, it seems that securing all merits including convenient preparations of samples with large areas, low costs, multiple abundant hot spots of uniform distributions, excellent repeatibilities, and strong enhanced performances does embrace a certain degree of difficulties.

In the present experimental and simulative work, we design periodic light-trapped nanocavities by utilizing the abundantly reserved Al material. Via periodic light-trapped nanocavities, abundant light energy can be localized inside these nanocavities, in which the contained energy manages to re-amplify hot spots on the Al film, leading to the acquisition of an enhanced effect and the suitability for SERS substrates of structured nanoarrays in the UV area. The sample area can size up to the decimeter level, and the enhancement factor of

Received: June 28, 2021

Revised: July 12, 2021

Published: July 28, 2021



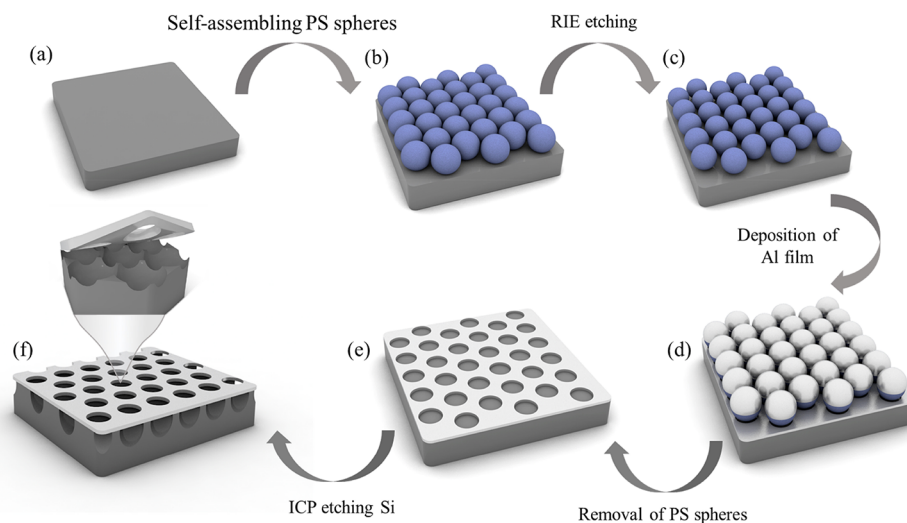


**Figure 1.** Schematic illustration of fabricating light-trapped nanocavities. (a) Si wafer after the cleaning process, (b) self-assembly of monolayered PS arrays, (c) PS templates after RIE, (d) PS templates with the deposition of the Al film (e) templates after stripping away the PS arrays, and (f) Finally finished templates with imbedded nanocavities after Si is etched by ICP under the Al film.

repetitive Raman signals from adenine molecules reaches greater than  $10^6$ , which qualifies as the international advanced level.

## METHODS

**Materials.** Monodispersed polystyrene nanospheres (10 wt % aqueous solution), with a diameter of 500 nm, were purchased from Bangs Laboratories. For UV-SERS experiments, adenine with a purity of 99.0% was bought from Innochem Co., Ltd. Single crystalline silicon wafers (100) obtained from Giant Electronic Optical (Zhe Jiang) Co., Ltd. were used for the sample preparation.

**Self-Assembly of PS Arrays.** Silicon wafers were ultrasonically cleaned in deionized water, acetone, and ethanol for 6 min prior to being immersed in piranha solution ( $\text{H}_2\text{SO}_4:\text{H}_2\text{O}_2 = 3:1$  volume ratio) with 240 °C boiling for half an hour and then being washed by deionized water several times. When the cleaning was finished, these silicon wafers were stored in sodium lauryl sulfate solution for further use. The mixed solution of 240  $\mu\text{L}$  of PS solution and 250  $\mu\text{L}$  of ethanol was prepared and sonicated for 30 s in a microcentrifuge tube. Afterward, the diluted PS solution was removed into a 5 mL injector ready for the next step.

At the initial stage in the self-assembly process, two cleaned silicon wafers were placed into the Petri dish in different places, with the first one at the bottom of the Petri dish acting as a supporting template while the other one on the edge with a tilt angle of 45° acting as an auxiliary role in the experiment. Afterward, deionized water was slowly added into the Petri dish till the waterline exactly reached the tilted silicon wafer. The injector with the prepared PS solution was then fixed on an injection pump, whereas the syringe needle of the injector was placed adjacently. In the following steps, the injection rate was adjusted and the tilted silicon wafer was used as a supporting platform, such that each drip of the solution was homogeneously dispersed on the water surface. After a PS monolayer thin film that floated on the water surface was observed, the injection pump can be turned off. Thereafter, a peristaltic pump was operated at a speed of 11 mL/min for 4 h, aiming to purify the PS monolayer film through exchanging the water under PS particles. This operation was followed by

pumping water (8 mL/min) until the monolayer PS film was totally settled on the first silicon wafer. Finally, it was stored at room temperature after the wafer was completely dried prior to the fabrication process.

**Probe Molecules.** We prepared 1 mM adenine aqueous solution in a centrifuge tube with ultrasonic heating at 50 °C for 30 min to ensure that the adenine powder was fully dissolved. Then, 20  $\mu\text{L}$  of adenine aqueous solution was measured to be drop-cast onto the surface of the sample until the droplets evaporated naturally.

**SEM.** A scanning electron microscope (SEM, Hitachi S-4800, Japan) was used to characterize the morphology of the prepared samples.

**Reflectance Spectra Characterization.** The reflectance spectra of arrays were recorded by an Avantes fiber spectrometer system (Avantes BV, Apeldoorn, Netherlands) with a reflection probe, which was fixed perpendicularly to the sample surface. Spectra were collected under an excitation power = 90 W, beam size = 2  $\mu\text{m}$ , and exposure time = 25 ms, and we used the reflectance spectra of a pure Al film as a reference spectrum.

**UV-SERS Measurements.** UV-SERS measurements were conducted by a microscopic confocal Raman system (LabRAM HR Evolution, HORIBA). The laser (excitation wavelength of 325 nm) was focused on the sample using an LMU-40X-NUV microscope objective (NA = 0.47), and UV-SERS signals were collected under an excitation power = 0.2 mW, acquisition time = 60 s, laser spot = 1  $\mu\text{m}$ , and gratings = 1800 gr/mm.

**FDTD (Finite-Difference Time-Domain) Solutions.** Simulations based on the 3D FDTD numerical method (Lumerical Solutions, Canada) using Yee cells were carried out to study the 325 nm optical properties of the light-trapped nanocavity system. A normal incident plane wave with polarization along the  $x$ -axis was used as the light source. In the entire simulation process, a perfectly matched-layer boundary condition along the  $z$ -direction and a periodic boundary condition along the  $x$ - and  $y$ -axes were prescribed. To ensure both the convergence and the accuracy, we set the simulation time to 1000 fs and the Yee-cell size to 1 nm.

Being retrieved from simulations, the refractive index in terms of the PS colloid spheres equaled 1.585, and the optical

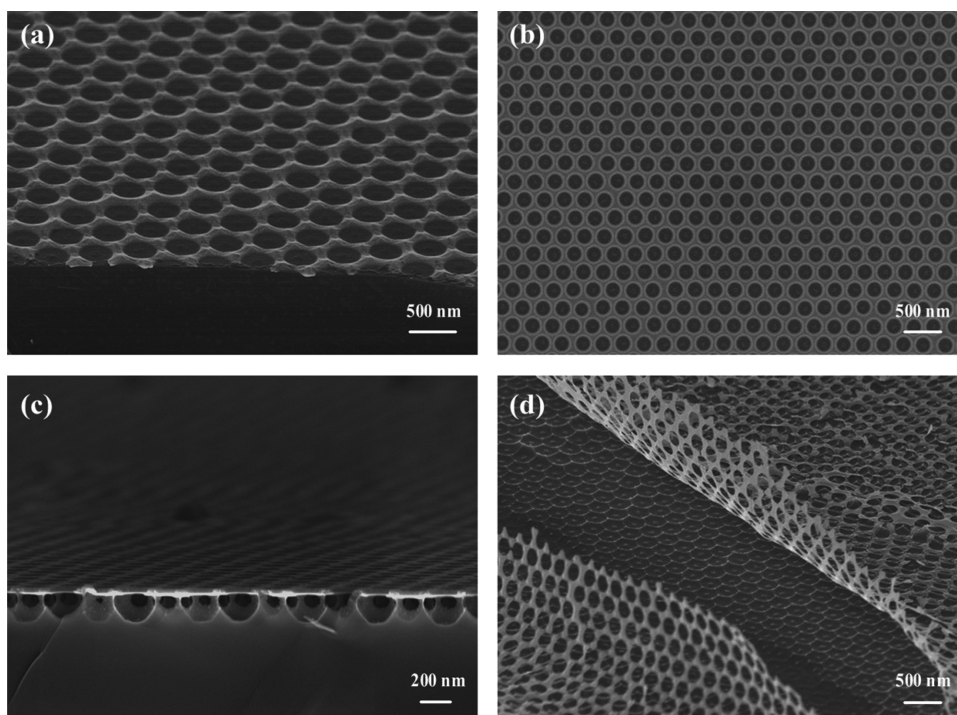


**Figure 2.** Representative SEM images of Al nanostructures with a fixed period of 500 nm and an average diameter of 350 nm. (a) Cross-section view of Al nanovoids (without ICP etching on Si). (b) Top view of nanocavities. (c) Cross-section view of nanocavities. (d) Cross-section view of nanocavities. Si cavities can be clearly seen after the upper Al film is lifted.

parameters of aluminum and silicon were listed in the software material database. Finally, the electromagnetic field enhancement was post-processed by  $\log(E_{\text{loc}}/E_0)^4$ , where  $E_{\text{loc}}$  and  $E_0$  represent the localized electric field and the incident electric field, respectively.

## RESULTS AND DISCUSSION

**Preparation and Morphological Characterization.** In Figure 1a–f, we feel obligated to first describe the construction of the nanostructure, which constitutes an essential part of the proposed work. Polystyrene (PS) arrays fabricated by nanosphere lithography were utilized as supporting templates. These templates were subsequently etched by reactive ion etching (RIE) for 30 s, aiming to adjust the size of PS spheres with an etching rate approximately equal to 5 nm/s. Next, these pre-etched templates were placed in an electric beam evaporation system (aTEMD-500 China), where thin Al films (50 nm) were deposited onto the PS templates under a high vacuum of  $9.9 \times 10^{-4}$  Pa and a deposition rate of 4 Å/s.

Afterward, these templates experienced a stripping process by using thermal conductive tape, indicating that PS spheres could be totally peeled off. Eventually, an inductively coupled plasma (ICP Sentech Germany) etching device was used to etch Si substrates.

Actually, geometrical features of light-trapped nanocavities can be tuned by changing the lattice parameter, the diameter of PS spheres, the thickness of Al films, and the depth of Si cavities. In this work, our favorite modulation is based on the depth of Si cavities. The depth ranges from 100 to 400 nm with an increment of 100 nm. These Si nanocavities formed by ICP etching with antireflective capability can enhance the absorption of the incident light on the Al film. For the purpose of comparison, Al nanovoid samples were designed to demonstrate our light-trapped nanocavity properties.

In Figure 2, both nanovoids and nanocavities exhibit a high degree of homogeneity in a large area, and the overall standard deviation of the diameter is 1.738 nm, thus achieving uniform and reproducible responses. The top view of hexagonal nanocavities is shown in Figure 2b. From the cross-section image in Figure 2c, conspicuous orderly Si cavities are observed under Al films compared to Figure 2a, indicating that Al nanovoids have not undergone an ICP process. Here, we show only the most representative nanocavities with 300 nm etching depth that look nearly hemispherical cross-sectional-wise. Incidentally, the images of those small ghost-looking circles result from the silhouette of the rugged cross section shown in the inset of Figure 1f. For the purpose of fully presenting the structure and morphology, a cross-section SEM image of nanocavities with the upper Al film lifted is shown in Figure 2d, which exhibits the high ductility of the Al film.

**Optical Characterization.** Far-field spectral reflectance is also systematically measured in Figure 3. By adjusting ICP etching depths (from 0 to 400 nm), the short-wavelength plasmonic resonances can be tuned under normal incidence. A vertical dotted line is exactly located at 325 nm, indicating the Raman excitation wavelength. It can be seen that both the spectra of without ICP etching and with 100 nm ICP etching display no resonance dip between 300 and 350 nm, but with a weak resonance at about 250 nm in the 100 nm ICP etching system. In the case of 200 nm etching depths, however, the resonance peak intensity increases and the resonance wavelength shifts toward longer wavelengths at around 287 nm. As ICP etching depths increase to 300 nm, the resonance wavelength further red-shifts, with a resonance peak centered in the vicinity of 338 nm, which is located near the experimental 325 nm Raman laser source. After further etching to 400 nm, the resonance peak in the ultraviolet region disappears. It is worth noting that the SPR mode is considered

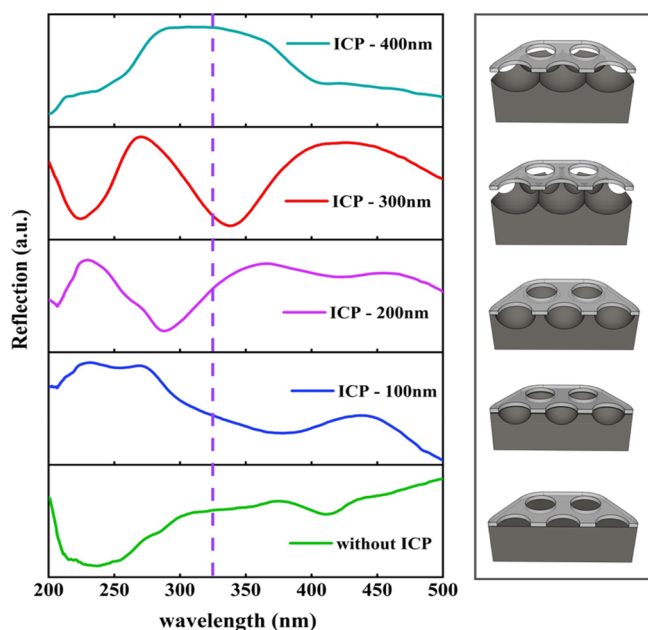


**Figure 3.** Reflectance spectra of light-trapped nanocavities at normal incidence with different ICP etching depths compared with no ICP etching. All of them acquired under 30 s RIE and a 50 nm Al film.

as a result of the coupling of the LSPR (localized surface plasmon resonance) mode, SPP mode, cavity mode, and lightning rod effect (to be shown in Figure 5).

**UV-SERS Effects.** We proceed to explore SERS capabilities of our light-trapped nanostructures in the ultraviolet region. Because molecules with absorption peaks exactly near 325 nm contribute to resonance Raman enhancements, we cannot clearly differentiate whether the enhanced Raman signal originates from SERS or from surface-enhanced resonance Raman scattering. Due to the fact that the electric absorption peaks of adenine<sup>35</sup> at 260 nm are situated far below our Raman laser source at 325 nm, here adenine molecules are intentionally chosen as the non-resonant Raman probes at 325 nm excitation. In addition, the deposition of adenine molecules on the substrate surface is mainly governed by physical adsorption. Therefore, no charge transfer<sup>36</sup> occurs, leading to little shift of the molecular absorption peak. As seen in Figure 4a,b, the SERS spectra obtained from the nanocavity systems clearly exhibit four prominent modes (1241, 1324, 1475, and 1590  $\text{cm}^{-1}$ ). UV-SERS peaks are compared with peaks of the resonant Raman spectrum of bulk adenine, and the comparison is discussed (see in the Supporting Information).

From Figure 4a, we compare the respective Raman spectra in terms of adenine adsorbed on nanostructured light-trapped nanocavities (with different ICP etching depths), Si substrates,

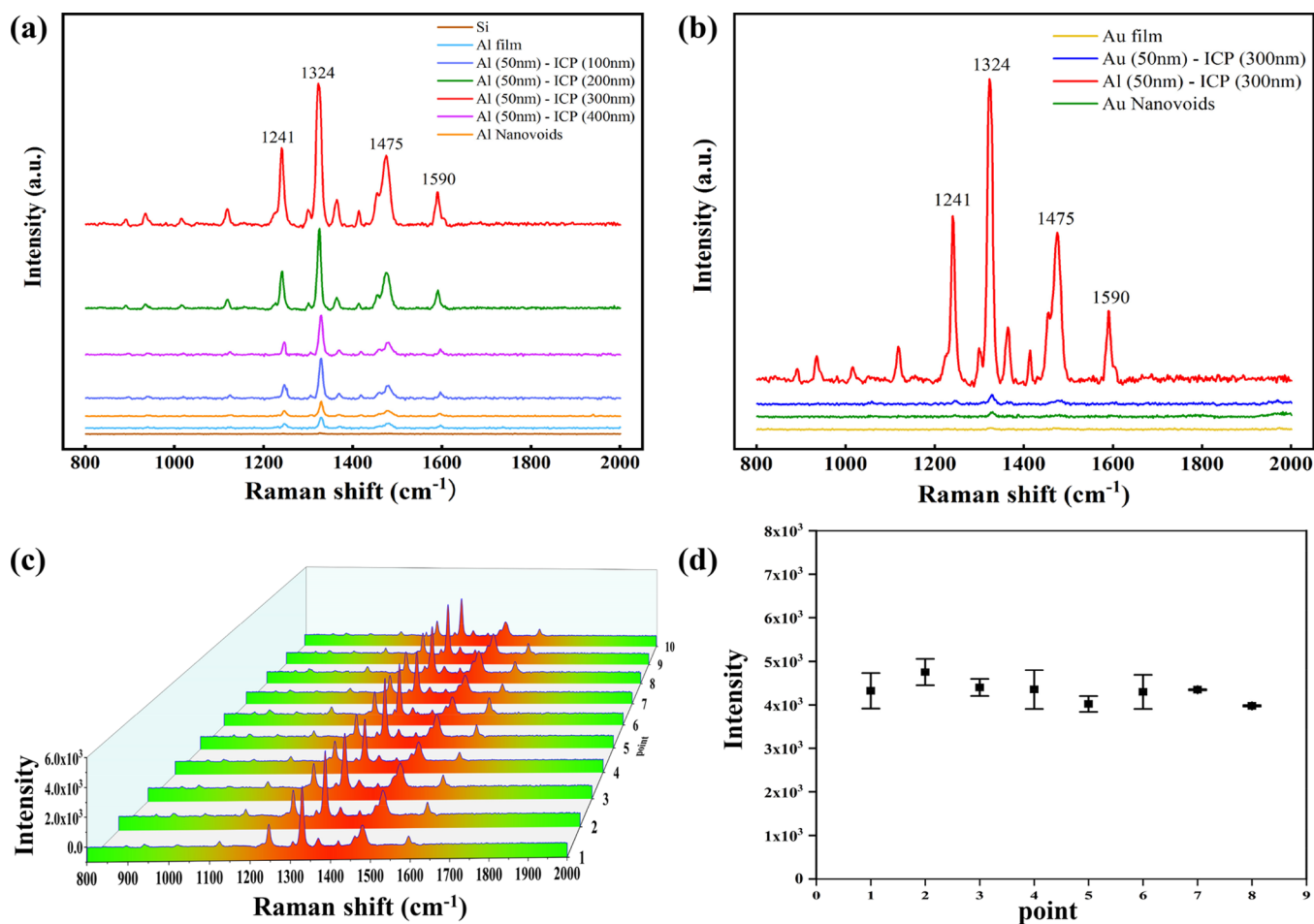


**Figure 4.** Raman spectra of adenine (1 mM) molecules adsorbed on substrates. (a) Al-based substrates, (b) Au-based substrates, and (c) the same light-trapped nanocavity sample at scattered points, (d) converting (c) into an intensity image.

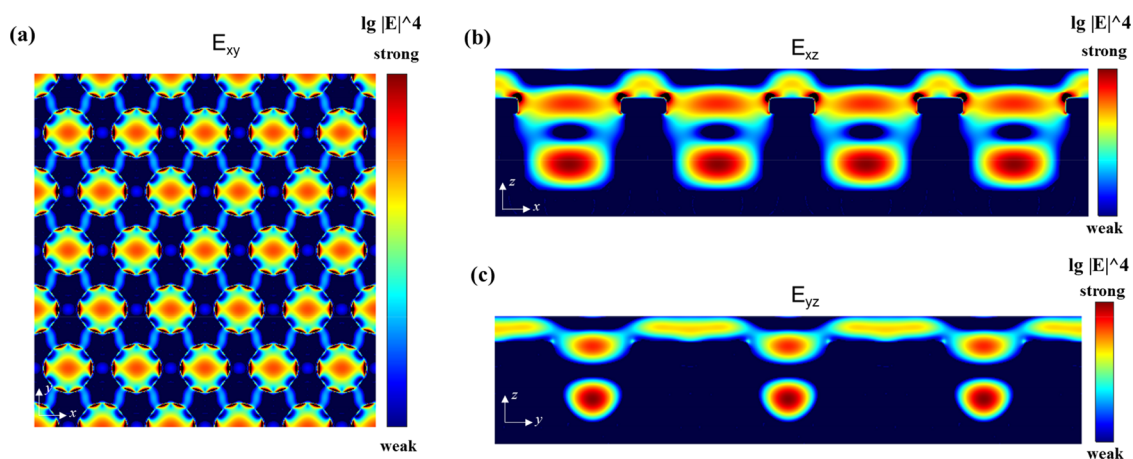


**Figure 5.** Simulation results of light-trapped nanocavities with structural dimensions: diameter = 350 nm, thickness of the Al film = 50 nm, and depths of Si nanocavities = 300 nm. (a) EM field distribution of the top surface. (b and c) Cross-sectional views of the EM field distributions.

and Al films as well as Al nanovoid architecture. Strikingly, the strongest peak at  $1324\text{ cm}^{-1}$  (stretching modes of various CN bonds of adenine)<sup>37</sup> appears prominent in the case of nanocavities at 300 nm ICP etching depth, namely, 13 times stronger than the pure aluminum film and 187 times that of the Si film. By contrast, the signal intensity of Al nanovoids is 9 times inferior to that of Al nanocavities, revealing more electromagnetic field enhancement regions inside this novel nanocavity structure. Furthermore, we explore SERS capabilities by changing the diameter size and Al film thickness. We find that substrates that experienced RIE for 30 s (diameter size = 350 nm) exhibit the strongest enhancement and substrates with a 50 nm Al film can be considered to have the optimal parameters (see Figures S4 and S5 in the Supporting Information for details).

To further verify the superior performance of this structure, we perform SERS experiments on Au-based systems under the same condition in Figure 4b. Then, we discover that arrays of Au nanocavities do not exhibit such a powerful enhancement ability in the UV region due to the loss produced by the presence of interband transitions<sup>38</sup> in the UV range. However, Au nanocavities continue to show stronger enhancements than the Au film, and these structured nanocavities may serve as better candidates for SERS substrates in the visible range. Therefore, these nanocavities may be ideally applied to other plasmonic materials. Meanwhile, Raman signals of adenine spectra display uniform distribution, as shown in Figure 4c,d, and scattered points from the same sample appeared to have similar intensities (between 4000 and 4700 counts), confirming the satisfactory homogeneity and reproducibility of Al nanocavities. We further demonstrate the SERS signal uniformity by performing the mapping of the substrate on a random area (see the result shown in Figure S3 in the Supporting Information). The calculated relative standard deviation (RSD) of the mapping result is approximately 10.26%.

The enhancement factor is accepted as the most direct parameter to measure the surface reinforcing effect. Therefore, we quantitatively estimate the SERS effect of substrates, and the SERS enhancement factor of Al light-trapped nanocavities is achieved to be  $1.3 \times 10^6$ , based on the  $1324\text{ cm}^{-1}$  mode (see the Supporting Information for details). Our results thus confirm the ability of light-trapped nanocavities for serving as high-performance SERS platforms in the UV region.

Simulations based on the FDTD numerical method are conducted to confirm this enhancement mechanism. In Figure 5, LSPR mode and SPP mode<sup>39,40</sup> on the Al–air interface, cavity mode in Si cavities, and the lightning rod effect on the edge of the nanohole clearly coexist to form a hybridized mode in the proposed system. Strong hot spots are effectively generated at the edge of the upper Al film. Interestingly, abundant hot spots successfully appear in such Si cavities below the Al film as we expected. In this case, the coexistence and the interaction of multiple modes yield the enhancement, indeed constituting a very complicated physical process. Truthfully, it is difficult to distinguish the contribution of each mode if the cavity mode generated inside the Si cavity, the LSPR mode generated in the nanohole, the SPP mode in periodic Al nanostructures, and the lightning rod effect on the edge of the nanohole are all included. However, by changing the depth of the cavity, the synergy and competition effect of several modes show a conspicuous SPR resonance peak near 325 nm of the far-field reflection spectrum, suggesting a large amount of concentrated energy conversion. Thus, by changing the structural parameters and then modulating the interaction between multiple modes, we finally achieve the purpose of regulating SPR. Moreover, the effect of alumina layers has been further analyzed in Figure S2 and we find that surface oxidation does not dramatically change the EM enhancement on such Al surfaces and inside Si cavities of light-trapped nanocavities.

## CONCLUSIONS

In this work, a method to enhance Raman signals by increasing the light-trapped capability has been developed. Through the combination of nanosphere lithography and the etching technique, ordered nanocavity arrays of large areas have been fabricated. The experimental enhancement factor has reached six orders of magnitude, and an excellent uniformity of SERS signals is achieved on the whole wafer. Moreover, the 3D finite-difference time-domain method is used to investigate near fields of light-trapped nanocavity-dependent plasmonic resonances and validate experimental results. This platform contributes significantly to potential applications of low-cost Al-based materials in UV-SERS detection, which can be promisingly adapted in the industrial manufacture of highly sensitive and reliable bio-sensing devices for applications within the UV region.

## ■ ASSOCIATED CONTENT

### SI Supporting Information

The Supporting Information is available free of charge at <https://pubs.acs.org/doi/10.1021/acs.jpcc.1c05175>.

Estimation of enhancement factors; calculation of converted depth (Figure S1); impact of the natural oxide layer on aluminum (Figure S2); SERS mapping image of the substrate (Figure S3); discussions on other parameters (Figures S4 and S5); correlated reflectance images (Figure S6); and UV-SERS peaks compared with peaks of resonant Raman spectrum of bulk adenine (PDF)

## ■ AUTHOR INFORMATION

### Corresponding Authors

**Guoya Sun** – Department of Physics, Collaborative Innovation Center for Optoelectronic Semiconductors and Efficient Devices, Jiujiang Research Institute, Xiamen University, Xiamen 361005, China; Email: [gysun@xmu.edu.cn](mailto:gysun@xmu.edu.cn)

**Zhilin Yang** – Department of Physics, Collaborative Innovation Center for Optoelectronic Semiconductors and Efficient Devices, Jiujiang Research Institute, Xiamen University, Xiamen 361005, China; [orcid.org/0000-0002-4799-1492](https://orcid.org/0000-0002-4799-1492); Email: [zlyang@xmu.edu.cn](mailto:zlyang@xmu.edu.cn)

### Authors

**Yue Zeng** – Department of Physics, Collaborative Innovation Center for Optoelectronic Semiconductors and Efficient Devices, Jiujiang Research Institute, Xiamen University, Xiamen 361005, China

**Renxian Gao** – Department of Physics, Collaborative Innovation Center for Optoelectronic Semiconductors and Efficient Devices, Jiujiang Research Institute, Xiamen University, Xiamen 361005, China

**Jingyu Wang** – Department of Physics, Collaborative Innovation Center for Optoelectronic Semiconductors and Efficient Devices, Jiujiang Research Institute, Xiamen University, Xiamen 361005, China

**Tien-Mo Shih** – Department of Mechanical Engineering, University of California, Berkeley, California 94720, United States

**Jiasheng Lin** – State Key Laboratory of Physical Chemistry of Solid Surfaces, iChEM, College of Chemistry and Chemical Engineering, Xiamen University, Xiamen 361005, China

**Yonglin He** – Department of Physics, Collaborative Innovation Center for Optoelectronic Semiconductors and Efficient Devices, Jiujiang Research Institute, Xiamen University, Xiamen 361005, China

**Jiawei Chen** – State Key Laboratory of Physical Chemistry of Solid Surfaces, iChEM, College of Chemistry and Chemical Engineering, Xiamen University, Xiamen 361005, China

**Da Zhan** – State Key Laboratory of Luminescence and Applications, Changchun Institute of Optics, Fine Mechanics and Physics, Chinese Academy of Sciences, Changchun 130033, China

**Jinfeng Zhu** – Institute of Electromagnetics and Acoustics, Xiamen University, Xiamen 361005, China; [orcid.org/0000-0003-3666-6763](https://orcid.org/0000-0003-3666-6763)

**Weimin Yang** – Department of Physics, Collaborative Innovation Center for Optoelectronic Semiconductors and Efficient Devices, Jiujiang Research Institute, Xiamen University, Xiamen 361005, China

**Peiwen Ren** – Department of Physics, Collaborative Innovation Center for Optoelectronic Semiconductors and Efficient Devices, Jiujiang Research Institute, Xiamen University, Xiamen 361005, China

**Fangfei Jiao** – Department of Physics, Collaborative Innovation Center for Optoelectronic Semiconductors and Efficient Devices, Jiujiang Research Institute, Xiamen University, Xiamen 361005, China

Complete contact information is available at: <https://pubs.acs.org/doi/10.1021/acs.jpcc.1c05175>

### Author Contributions

\*Y.Z. and R.G. contributed equally to this work.

### Notes

The authors declare no competing financial interest.

## ■ ACKNOWLEDGMENTS

This work was supported by the National Science Foundation of China (91850119 and 21673192), the MOST (2016YFA0200601 and 2017YFA0204902), and the Natural Science Foundation of Jiangxi Province of China (20192ACB20032). The authors would like to thank Dr. Yuejiao Zhang, Dr. Shaoxin Shen, Dr. Jie Zheng, Dr. Min Gao, Yifan Bao, and Qingqi Chen for helpful discussions. The authors would also like to thank the anonymous reviewer for constructive comments.

## ■ REFERENCES

- (1) Nie, S.; Emery, S. R. Probing single molecules and single nanoparticles by surface-enhanced Raman scattering. *Science* **1997**, *275*, 1102–1106.
- (2) Wu, T.; Li, K.; Zhang, N.; Xia, J.; Zeng, Q.; Wen, X.; Dinish, U. S.; Olivo, M.; Shen, Z.; Liu, Z.; Xiong, Q.; Luo, Y.; Maier, S. A.; Wei, L. Ultrawideband Surface Enhanced Raman Scattering in Hybrid Graphene Fragmented-Gold Substrates via Cold-Etching. *Adv. Opt. Mater.* **2019**, *7*, 1900905–1900909.
- (3) El-Khoury, P. Z.; Schultz, Z. D. From SERS to TERS and Beyond: Molecules as Probes of Nanoscopic Optical Fields. *J. Phys. Chem. C* **2020**, *124*, 27267–27275.
- (4) Park, S.-M.; Lee, K. S.; Kim, J.-H.; Yeon, G. J.; Shin, H.-H.; Park, S.; Kim, Z. H. Direct Visualization of Gap-Plasmon Propagation on a Near-Touching Nanowire Dimer. *J. Phys. Chem. Lett.* **2020**, *11*, 9313–9320.
- (5) Leong, S.; Koh, C. S. L.; Sim, H. Y. F.; Lee, Y. H.; Han, X.; Phan-Quang, G. C.; Ling, X. Y. Enantiospecific Molecular Fingerprinting Using Potential-Modulated Surface-Enhanced Raman Scattering to Achieve Label-Free Chiral Differentiation. *ACS Nano* **2021**, *15*, 1817–1825.
- (6) Pramanik, A.; Gao, Y.; Patibandla, S.; Mitra, D.; McCandless, M. G.; Fassero, L. A.; Gates, K.; Tandon, R.; Ray, P. C. Aptamer Conjugated Gold Nanostar-Based Distance-Dependent Nanoparticle Surface Energy Transfer Spectroscopy for Ultrasensitive Detection and Inactivation of Corona Virus. *J. Phys. Chem. Lett.* **2021**, *12*, 2166–2171.
- (7) Gwo, S.; Wang, C.-Y.; Chen, H.-Y.; Lin, M.-H.; Sun, L.; Li, X.; Chen, W.-L.; Chang, Y.-M.; Ahn, H. Plasmonic Metasurfaces for Nonlinear Optics and Quantitative SERS. *ACS Photonics* **2016**, *3*, 1371–1384.
- (8) Liu, Y.; Zhang, H.; Geng, Y.; Xu, S.; Xu, W.; Yu, J.; Deng, W.; Yu, B.; Wang, L. Long-Range Surface Plasmon Resonance Configuration for Enhancing SERS with an Adjustable Refractive Index Sample Buffer to Maintain the Symmetry Condition. *ACS Omega* **2020**, *5*, 32951–32958.

- (9) Ding, Q.; Wang, J.; Chen, X.; Liu, H.; Li, Q.; Wang, Y.; Yang, S. Quantitative and Sensitive SERS Platform with Analyte Enrichment and Filtration Function. *Nano Lett.* **2020**, *20*, 7304–7312.
- (10) Zhang, Y. J.; Chen, S.; Radjenovic, P.; Bodappa, N.; Zhang, H.; Yang, Z. L.; Tian, Z. Q.; Li, J. F. Probing the Location of 3D Hot Spots in Gold Nanoparticle Films Using Surface-Enhanced Raman Spectroscopy. *Anal. Chem.* **2019**, *91*, 5316–5322.
- (11) Li, J. F.; Huang, Y. F.; Ding, Y.; Yang, Z. L.; Li, S. B.; Zhou, X. S.; Fan, F. R.; Zhang, W.; Zhou, Z. Y.; Wu, D. Y.; et al. Shell-isolated nanoparticle-enhanced Raman spectroscopy. *Nature* **2010**, *464*, 392–395.
- (12) Gao, R.; Zhang, Y.; Zhang, F.; Guo, S.; Wang, Y.; Chen, L.; Yang, J. SERS polarization-dependent effects for an ordered 3D plasmonic tilted silver nanorod array. *Nanoscale* **2018**, *10*, 8106–8114.
- (13) Jin, X.; Zhu, Q.; Feng, L.; Li, X.; Zhu, H.; Miao, H.; Zeng, Z.; Wang, Y.; Li, Y.; Wang, L.; Liu, X.; Shi, G. Light-Trapping SERS Substrate with Regular Bioinspired Arrays for Detecting Trace Dyes. *ACS Appl. Mater. Interfaces* **2021**, *13*, 11535–11542.
- (14) Ward, D. R.; Grady, N. K.; Levin, C. S.; Halas, N. J.; Wu, Y.; Nordlander, P.; Natelson, D. Electromigrated nanoscale gaps for surface-enhanced Raman spectroscopy. *Nano Lett.* **2007**, *7*, 1396–1400.
- (15) Li, J.; Deng, T. S.; Liu, X.; Dolan, J. A.; Scherer, N. F.; Nealey, P. F. Hierarchical Assembly of Plasmonic Nanoparticle Heterodimer Arrays with Tunable Sub-5 nm Nanogaps. *Nano Lett.* **2019**, *19*, 4314–4320.
- (16) Belushkin, A.; Yesilkoy, F.; Altug, H. Nanoparticle-Enhanced Plasmonic Biosensor for Digital Biomarker Detection in a Microarray. *ACS Nano* **2018**, *12*, 4453–4461.
- (17) Liang, W.; Bockrath, M.; Bozovic, D.; Hafner, J. H.; Tinkham, M.; Park, H. Fabry - Perot interference in a nanotube electron waveguide. *Nature* **2001**, *411*, 665–669.
- (18) He, Z.; Qiu, W.; Kizer, M. E.; Wang, J.; Chen, W.; Sokolov, A. V.; Wang, X.; Hu, J.; Scully, M. O. Resolving the Sequence of RNA Strands by Tip-Enhanced Raman Spectroscopy. *ACS Photonics* **2021**, *8*, 424–430.
- (19) Gabel, M.; O'Callahan, B. T.; Groome, C.; Wang, C.-F.; Ragan, R.; Gu, Y.; El-Khoury, P. Z. Mapping Molecular Adsorption Configurations with <5 nm Spatial Resolution through Ambient Tip-Enhanced Raman Imaging. *J. Phys. Chem. Lett.* **2021**, *12*, 3586–3590.
- (20) Yuksel, S.; Ziegler, M.; Goerke, S.; Huebner, U.; Weber, K.; Schaaf, P.; Meyer, H. G.; Cialla-May, D.; Popp, J. Hierarchically-Designed 3D Flower-Like Composite Nanostructures as an Ultra-stable, Reproducible, and Sensitive SERS Substrate. *ACS Appl. Mater. Interfaces* **2017**, *9*, 38854–38862.
- (21) Sun, M.; Zhang, S.; Fang, Y.; Yang, Z.; Wu, D.; Dong, B.; Xu, H. Near - and Deep-Ultraviolet Resonance Raman Spectroscopy of Pyrazine-Al<sub>4</sub> Complex and Al<sub>3</sub>-Pyrazine-Al<sub>3</sub> Junction. *J. Phys. Chem. C* **2009**, *113*, 19328–19334.
- (22) Yang, Z.; Li, Q.; Fang, Y.; Sun, M. Deep ultraviolet tip-enhanced Raman scattering. *Chem. Commun.* **2011**, *47*, 9131–9133.
- (23) Tian, Z. Q.; Ren, B. Adsorption and reaction at electrochemical interfaces as probed by surface-enhanced Raman spectroscopy. *Annu. Rev. Phys. Chem.* **2004**, *55*, 197–229.
- (24) Wu, D. Y.; Li, J. F.; Ren, B.; Tian, Z. Q. Electrochemical surface-enhanced Raman spectroscopy of nanostructures. *Chem. Soc. Rev.* **2008**, *37*, 1025–1041.
- (25) Cui, L.; Mahajan, S.; Cole, R. M.; Soares, B.; Bartlett, P. N.; Baumberg, J. J.; Hayward, I. P.; Ren, B.; Russell, A. E.; Tian, Z. Q. UV SERS at well ordered Pd sphere segment void (SSV) nanostructures. *Phys. Chem. Chem. Phys.* **2009**, *11*, 1023–1026.
- (26) Ren, B.; Lin, X. F.; Yang, Z. L.; Liu, G. K.; Aroca, R. F.; Mao, B. W.; Tian, Z. Q. Surface-enhanced Raman scattering in the ultraviolet spectral region: UV-SERS on rhodium and ruthenium electrodes. *J. Am. Chem. Soc.* **2003**, *125*, 9598–9599.
- (27) Zheng, J.; Yang, W.; Wang, J.; Zhu, J.; Qian, L.; Yang, Z. An ultranarrow SPR linewidth in the UV region for plasmonic sensing. *Nanoscale* **2019**, *11*, 4061–4066.
- (28) Li, Z.; Li, C.; Yu, J.; Li, Z.; Zhao, X.; Liu, A.; Jiang, S.; Yang, C.; Zhang, C.; Man, B. Aluminum nanoparticle films with an enhanced hot-spot intensity for high-efficiency SERS. *Opt. Express* **2020**, *28*, 9174–9185.
- (29) Sharma, B.; Cardinal, M. F.; Ross, M. B.; Zrimsek, A. B.; Bykov, S. V.; Punihaole, D.; Asher, S. A.; Schatz, G. C.; Van Duyne, R. P. Aluminum Film-Over-Nanosphere Substrates for Deep-UV Surface-Enhanced Resonance Raman Spectroscopy. *Nano Lett.* **2016**, *16*, 7968–7973.
- (30) Yang, R.; Cheng, Y.; Sun, M. Aluminum plasmon-enhanced deep ultraviolet fluorescence resonance energy transfer in h-BN/graphene heterostructure. *Opt. Commun.* **2021**, *498*, 127224.
- (31) Jha, S. K.; Ahmed, Z.; Agio, M.; Ekinci, Y.; Löffler, J. F. Deep-UV surface-enhanced resonance Raman scattering of adenine on aluminum nanoparticle arrays. *J. Am. Chem. Soc.* **2012**, *134*, 1966–1969.
- (32) Su, D.; Jiang, S.; Yu, M.; Zhang, G.; Liu, H.; Li, M. Y. Facile fabrication of configuration controllable self-assembled Al nanostructures as UV SERS substrates. *Nanoscale* **2018**, *10*, 22737–22744.
- (33) Sigle, D. O.; Perkins, E.; Baumberg, J. J.; Mahajan, S. Reproducible Deep-UV SERS on Aluminum Nanovoids. *J. Phys. Chem. Lett.* **2013**, *4*, 1449–1452.
- (34) Ding, T.; Sigle, D. O.; Herrmann, L. O.; Wolverson, D.; Baumberg, J. J. Nanoimprint lithography of Al nanovoids for deep-UV SERS. *ACS Appl. Mater. Interfaces* **2014**, *6*, 17358–17363.
- (35) Barbatti, M.; Aquino, A. J. A.; Lischka, H. The UV absorption of nucleobases: semi-classical ab initio spectra simulations. *Phys. Chem. Chem. Phys.* **2010**, *12*, 4959–4967.
- (36) Tarakeshwar, P.; Palma, J. L.; Finkelstein-Shapiro, D.; Keller, A.; Urdaneta, I.; Calatayud, M.; Atabek, O.; Mujica, V. SERS as a Probe of Charge-Transfer Pathways in Hybrid Dye/Molecule-Metal Oxide Complexes. *J. Phys. Chem. C* **2014**, *118*, 3774–3782.
- (37) Giese, B.; McNaughton, D. Surface-enhanced Raman spectroscopic and density functional theory study of adenine adsorption to silver surfaces. *J. Mater. Chem. B* **2002**, *106*, 101–112.
- (38) Zhou, L.; Swearer, D. F.; Zhang, C.; Robotjazi, H.; Zhao, H.; Henderson, L.; Dong, L.; Christopher, P.; Carter, E. A.; Nordlander, P.; et al. Quantifying hot carrier and thermal contributions in plasmonic photocatalysis. *Science* **2018**, *362*, 69–72.
- (39) Liu, B. W.; Chen, S.; Zhang, J. C.; Yao, X.; Zhong, J. H.; Lin, H. X.; Huang, T. X.; Yang, Z. L.; Zhu, J. F.; Liu, S.; et al. A Plasmonic Sensor Array with Ultrahigh Figures of Merit and Resonance Linewidths down to 3 nm. *Adv. Mater.* **2018**, *30*, 1–7.
- (40) Ebbesen, T. W.; Lezec, H. J.; Ghaemi, H. F.; Thio, T.; Wolff, P. A. Extraordinary optical transmission through sub-wavelength hole arrays. *Nature* **1998**, *391*, 667–669.